Master of Science Thesis

SIMIND Based Pinhole Imaging

*

Development and Validation

Kurt Sundin

Supervisor: Michael Ljungberg, PhD

Medical Radiation Physics
Clinical Sciences, Lund
Lund University, 2006

ABSTRACT

The Monte Carlo method has become increasingly used to simulate imaging systems like the scintillation camera and SPECT systems. In order to investigate intrinsic properties of SPECT systems the Monte Carlo based application SIMIND (Simulating Medical Imaging Nuclear Detectors) has been developed. Up to now, it has not been able to simulate a pinhole-imaging device with SIMND. The aim of this work was therefore to develop such an application. The application has been developed for pinhole-imaging devices that consist of a knife-edge-shaped pinhole insert and a conical shielding device.

The pinhole collimator routine, developed in FORTRAN, tracks the path of each photon through the pinhole collimator during a simulation session. As a photon moves through the pinhole collimator, the routine registers if the photon passes through the aperture, penetrates trough the edge of the aperture or if the photon scatters in the pinhole collimator. This makes it possible to calculate fractions of geometrical, penetrating and scattered photons that contribute to an image generated by the simulation application, which is impossible in the real case.

Results from the constructed pinhole collimator routine were validated by comparing results from simulations with results obtained from experimental studies on a SPECT system with a pinhole collimator. Comparisons were also conducted with results from previously published characteristics of pinhole-imaging devices. The comparisons showed good agreement but with some differences in the values of the fraction of geometrical, penetrating and scattered photons compared to previously reported results.

CONTENT

INTRODUCTION

Monte Carlo techniques have proved to be very useful when investigating statistical processes. In Medical Radiation Physics, it is particularly useful to use Monte Carlo techniques to simulate transport and interaction of radiation in matter, i.e. penetration and scattering of photons and electrons. Applications are here found in all fields (nuclear medicine, radiology, radiotherapy, radiation protection and dosimetry). Monte Carlo simulation techniques have been widely used to simulate different medical imaging devices that involve photon radiation, such as the scintillation camera, SPECT (Single-Photon Emission Computed Tomography) and PET (Positron Emission Tomography) systems.

An advantage with simulation techniques as compared to experimental measurements is that a change of the geometry of the imaging device is often easy to make and it is easy to model different materials of the imaging device. Therefore, simulation techniques can be useful when developing or improving an imaging device. Another advantage with simulation techniques is that combined inseparable effects that contribute to the formation of an image are possible to separate, thus allowing for intrinsic properties of the device in question to be investigated. Monte Carlo simulations techniques are also very useful for educational purposes and provide a good way to teach how different imaging systems behave and what are their advantages and disadvantages.

At the Department of Medical Radiation Physics at Lund University, the Monte Carlo program SIMIND (Simulating Medical Imaging Nuclear Detectors) has been developed for many years and it has proved to be very useful for investigating nuclear medicine imaging system based on the scintillation camera. SIMIND is written in the FORTRAN 90 programming language and it simulates a standard clinical scintillation camera with SPECT. Up to now, the program has only included multi-hole collimators, such as the parallel-hole collimator.

The aim of this work was therefore to develop a pinhole collimator routine for the Monte Carlo simulation program SIMIND. With a developed SIMIND based pinhole collimator routine it will be possible to investigate different properties of such a small-object imaging system.

A pinhole collimator together with a scintillation camera is used for either SPECT or planar imaging of small objects. The pinhole collimator consists of two parts: a shielding device that protects the scintillation crystal from mechanical forces and background radiation, and a pinhole insert that can be either knife-edge-shaped or channelled. The inner surface of a knife-edge pinhole insert is shown in Figure 1. It has the shape of two opposite cones, one that

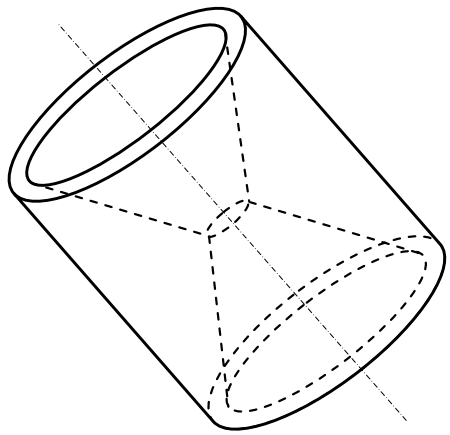

Figure 1. Above is an illustration of a knife-edge pinhole insert. The diameter of the aperture is usually in the order of some millimetres and the openings are of the order of some centimetres.

opens towards the object and one that opens towards the camera head. The intersection points between the two cones compose a small hole called aperture through which the radiation can pas. Instead of the knife-edge intersection, the two cones can intersect through a channel. In this case, the pinhole insert is called channelled. Compared to a channelled insert, with the same aperture diameter, the knife-edge insert has les spatial resolution but higher angle-dependent sensitivity. In this work, a knife-edge pinhole insert will be described. The reason for describing a knife-edge pinhole insert was that it was possible to access a knife pinhole insert at Lund University, which could be used when performing measurements to validate the constructed routine.

The photon radiation from the object will either:

- pass through the aperture of the knife-edge pinhole insert,
- penetrate through the edge of the aperture or
- scatter in the material of the knife-edge pinhole insert or the shielding material.

The penetrating and the scattered photons that contribute to the formation of an image will degrade the quality of the image (mainly by reducing the spatial resolution and the image contrast) and are therefore undesirable. By simulating a pinhole collimator with a Monte Carlo program, fractions such as number of photons that have passed geometrically through the aperture, penetrated the edge of the aperture or have scattered in the pinhole collimator can be calculated. Such information is important when optimizing the design of new pinhole collimators for different types of radionuclides and investigation methods or when developing correction methods for e.g. photon attenuation or scatter correction. Monte Carlo simulations of the imaging device are therefore useful to perform during such a development.

When comparing to the parallel-hole collimator, the advantage of the pinhole collimator is its high spatial resolution for small objects. There are other imaging devices, for example PET systems, that have higher spatial resolution than the pinhole collimator. However, since the scintillation camera is such a common device in medical clinics and there are different radiopharmaceutical agents suitable for investigations with the scintillation camera, the pinhole collimator is often the best alternative when requiring high resolution.

Because its high resolution for small objects the pinhole collimator is primarily used for small organs, such as the human thyroid, or for small-animal imaging e.g. rats or mice. A small object can be placed close to the aperture, creating a large magnification, but still be kept in the field-of-view of the pinhole collimator. The magnification of the pinhole collimator is a function of the focal length of the pinhole collimator and the distance between the aperture and the object and it increases as the object is brought closer to the pinhole collimator. The magnification compensate for the limitation of resolution that is caused by the limitation of the intrinsic resolution of the detector. The resolution of the pinhole collimator also depends on the diameter of the aperture, and the fraction of photons that penetrate through the edge of the aperture (Deloar 2003). Furthermore, the number of photons that penetrate the edge of the aperture depends on the acceptance angle of the pinhole collimator (Smith 1997), the pinhole collimator material (Tenny 1999) and the photon energy. The effect of these three parameters upon the spatial resolution is possible to investigate in detail with the in this work developed SIMIND pinhole collimator routine.

The main disadvantage of the pinhole collimator is a low counting sensitivity (cps/MBq) and that the sensitivity is angle dependent. This makes it difficult to acquire quantitative studies with high accuracy and correction for the angle-dependent sensitivity (Smith 1997) must be applied on the data set.

MATERIAL AND METHODS

Definition of the pinhole collimator

The geometry of a pinhole collimator can be separated into two major parts:

- the shielding device that protects the scintillation crystal from background radiation and mechanical forces and
- the pinhole insert with the aperture.

The shielding device usually has the shape of either a pyramid or a cone and it is mostly made of lead. The pinhole insert can be either the knife-edge type or a channelled type and the insert is often made of tungsten. The inner surface of the knife-edge pinhole insert consists of two cones where one is facing towards the object and the other one is facing towards the camera head. The small hole at the location where the two cones intersect is denoted the "aperture". In contrast to the sharp edge in a knife-edge pinhole insert, a channelled pinhole insert has a tubular channel between the two cones. The pinhole insert is attached to the shielding device by screwing it on to the top of the shielding device and it has therefore been threaded. Figure 2 shows a picture of a knife-edge pinhole insert where the aperture, the cone facing the object and the thread of the knife-edge pinhole insert can be seen.

Figure 2. A knife-edge pinhole insert.

In this work, a development of a simulation code based on a conical shielding device with a knife-edge pinhole insert is described. The following equation was used to describe the pinhole collimator, with its axis of symmetry orientated along the z-axis (towards the scintillation camera), mathematically in Cartesian coordinates

$$x^2 + y^2 = R^2(|h - h_0|) . \quad (1)$$

Here, R is the radius of a cone at a distance h from its apex h_o. To use Equation 1 in the actual simulation routine the geometry of the pinhole collimator was described by five compartments, as in the text below are denoted as C1-C5 as shown in Figure 3. C1 is the space defined by $z < z_1$, C2 is the space defined by $z_1 \leq z < z_2$, C3 is defined by $z_2 \leq z < z_3$, C4 is the space defined by $z_3 \leq z \leq z_4$ and C5 is the space defined by $z_4 < z$.

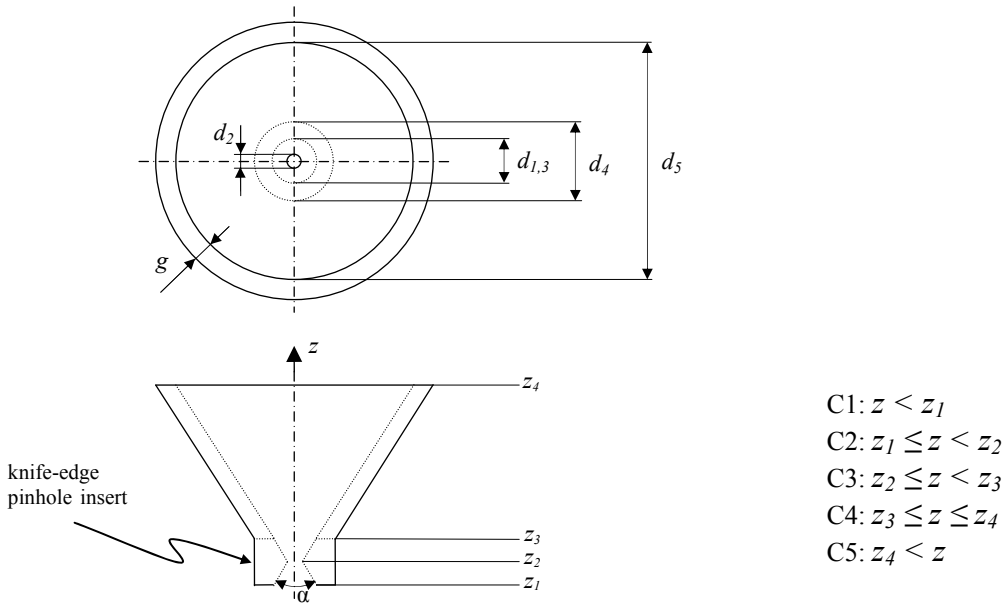

Figure 3. The figure illustrates how the pinhole collimator was subdivided into five different compartments along the *z*-axis**.** The different diameters of the pinhole collimator are also defined in the figure and the thickness (projected on to the *xy*-plane) of the wall of the shielding device is defined as g. The opening of the knife-edge pinhole insert is defined by the acceptance angle α.

The radius *R* of the different parts of the pinhole collimator was derived from geometrical considerations shown in Figure 3. For the lower part of the knife-edge pinhole insert (C2) the radius, R_1, of the inner surface was derived as

$$R_1 = \frac{z_2 - z}{z_2 - z_1}\left(\frac{d_1}{2} - \frac{d_2}{2}\right) + \frac{d_2}{2} \qquad z_1 \leq z < z_2 \tag{2}$$

where z_1 and z_2 are the lower and the upper boundaries of C2, respectively, in the z-direction, d_1 is the diameter of the entrance hole and d_2 is the diameter of the exit hole, i.e. the aperture. For the upper part of the knife-edge pinhole insert (C3) the radius, R_2, of the inner surface of the knife-edge pinhole insert was derived as

$$R_2 = \frac{z - z_2}{z_3 - z_2}\left(\frac{d_3}{2} - \frac{d_2}{2}\right) + \frac{d_2}{2} \qquad z_2 \leq z < z_3 \tag{3}$$

where z_2 and z_3 are the lower and the upper boundaries of C3, respectively, in the z-direction, d_2 is the diameter of the aperture and d_3 is the diameter of the exit hole, i.e. the hole towards the shielding device. The screw thread of the pinhole insert (C2 and C3) was not included in the geometrical description of the pinhole collimator. The outer surface of the knife-edge pinhole insert was described as a flat surface by the equation

$$x^2 + y^2 = \left(\frac{d_4}{2}\right)^2 \qquad z_1 \leq z < z_3 \tag{4}$$

were d_4 is the diameter of the rim of the knife-edge pinhole insert.

The radius, R_3, of the inner surface the of the conical shielding device (C4) was derived as

$$R_3 = \frac{z - z_3}{z_4 - z_3}\left(\frac{d_5}{2} - \frac{d_3}{2}\right) + \frac{d_3}{2} \qquad z_3 \leq z \leq z_4 \tag{5}$$

where z_3 and z_4 are the lower and upper boundaries of C4, respectively, in the z-direction, d_5 is the diameter of the exit hole towards the camera head and d_3 is the diameter of the entrance hole, i.e. the opening towards the knife-edge pinhole insert. The radius, R_4, of the outer surface of the shielding device was calculated by adding the thickness of its wall, projected onto the *xy*-plan, to the radius of its inner surface, that is

$$R_4 = \frac{z - z_3}{z_4 - z_3}\left(\frac{d_5}{2} - \frac{d_3}{2}\right) + \frac{d_3}{2} + g \qquad z_3 \le z \le z_4 . \tag{6}$$

Here, g is the thickness of the wall of the shielding device, projected onto the *xy*-plane.

With the different radii derived above together with Equation 1 and Equation 4 was it possible to define a number of sets that describe the inner and the outer space of the different parts of the pinhole collimator, i.e. the lower and the upper part of the knife-edge pinhole insert and the shielding device. The inner space of the lower part of the knife-edge pinhole insert was defined by the set

$$\left\{(x,y,z):\ \ z_1 \le z < z_2 \ \ \wedge \ \ x^2 + y^2 < R_1^2\right\} \tag{7}$$

and the inner space of the upper part of the knife-edge pinhole insert was defined by the set

$$\left\{(x,y,z):\ \ z_2 \le z < z_3 \ \ \wedge \ \ x^2 + y^2 < R_2^2\right\}. \tag{8}$$

The inner space of the shielding device was defined by the by set

$$\left\{(x,y,z):\ \ z_3 \le z \le z_4 \ \ \wedge \ \ x^2 + y^2 < R_3^2\right\}. \tag{9}$$

By comparing the position of a photon with the sets given above, Equations 7-9, it was possible to determine if the photon was inside the pinhole collimator or not. The outer space of the lower part of the knife-edge pinhole insert was defined by the set

$$\left\{(x,y,z):\ \ z_1 \le z < z_2 \ \ \wedge \ \ x^2 + y^2 > \left(\frac{d_4}{2}\right)^2\right\} \tag{10}$$

and the outer space of the upper part of the knife-edge pinhole insert was defined by the set

$$\left\{(x,y,z):\ \ z_2 \le z < z_3 \ \ \wedge \ \ x^2 + y^2 > \left(\frac{d_4}{2}\right)^2\right\}. \tag{11}$$

The outer space of the shielding device was defined by the set

$$\left\{(x,y,z):\ \ z_3 \le z \le z_4 \ \ \wedge \ \ x^2 + y^2 > R_4^2\right\}. \tag{12}$$

By comparing the position of a photon with the sets given above, Equations 10-12, it was possible to determine whether the photon was outside the pinhole collimator or not.

The sets above, defined by the Equations 7-12, were used in the pinhole collimator routine to determine if the location of the photon was inside or outside the different parts of the pinhole collimator. If the photon neither was located inside nor outside the different parts of the pinhole collimator, it was assumed that the photon was located inside the material of the pinhole collimator provided that the photon was not located inside C1 or C5.

The SIMIND Monte Carlo Code

SIMIND (Simulating Medical Imaging Nuclear Detectors) is a Monte Carlo program that simulates a standard clinical scintillation camera. SIMIND can be used with either Linux or Windows systems. To make a simulation faster several variance techniques are used in SIMIND, fore example forced interaction and detection techniques (Ljungberg 1998).

The CHANGE program allows the user to define the imaging system from a graphical user interface, like the window in shown Figure 4. The graphical user interface is launched from

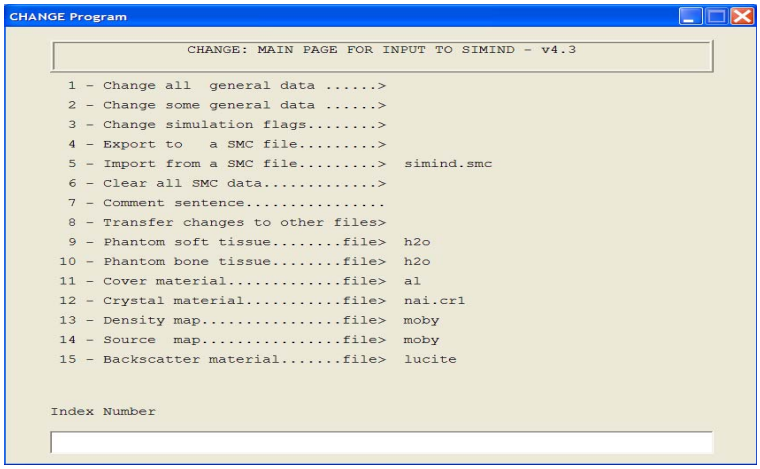

Figure 4. The main menu that appears on the screen when the change program is launched.

the command prompt by typing "change". The first window that appears on the screen is the main menu, shown in Figure 4. From the main menu, it is possible to select different windows and thereby access all the system parameters that SIMIND provides.

The SIMIND program is executed by giving the command "simind" followed by the name of a desired system file, defined with the CHANGE program, at the command prompt.

For a complete description of the SIMIND and the CHANGE program, the reader is referred to the SIMIND manual[1].

Pinhole collimator parameters, such as focal length, aperture diameter and acceptance angle, are not defined in CHANGE program in this version of the pinhole collimator routine. This is will be done later on.

The pinhole collimator routine is constructed as a subroutine to the SIIMND program. The pinhole collimator routine gives a geometrical description of the pinhole collimator and calculates the path through the pinhole collimator for each photon in a simulation session.

It is possible to define different types of radioactive sources with the CHANGE program. In the case of the pinhole collimator routine, the photons that are emitted from a sampled decay location are limited in direction to a cone centred on the mid-point of the entrance hole of the knife-edge pinhole insert, a variance technique referred to as forced detection. The position of the photon within the cone is given by three-dimensional Cartesian coordinates. The starting position of the photon when invoking the pinhole collimator routine has a *z*-coordinate that is equal to the distance, projected on to the z-axis, between the photon source and the plane to which the entrance hole of the knife-edge pinhole insert belongs, that is the value of z_1 in Figure 3.

The direction in space of the photon can be defined by the, so-called, direction cosines *(u,v,w)*. If a photon has travelled a distance *d* from its last position *(x',y',z')* then the new position of the photon *(x,y,z)* can be calculated from the direction cosines by multiplying these

[1] The SIMIND manual can be found at the web page: http://www.radfys.lu.se/simind/Manual.html

with the path length of the photon, the value of *d*, and add the result to the last position of the photon. The new position of the photon is then given by

$$\begin{cases} x = x' + d \cdot u \\ y = y' + d \cdot v \\ z = z' + d \cdot w \end{cases} . \qquad (13)$$

To simplify the code it was assumed that the photon did not interact with the air that surrounds the material of the pinhole collimator. This assumption implies that the direction of a photon can only change if the photon interacts with the material of the pinhole collimator.

A photon that strikes the pinhole collimator possesses a particular probability to interact with material of the pinhole collimator. The types of interactions that can occur are photo absorption, Compton scattering or coherent scattering. In addition to the probability to interact with the material of the pinhole collimator, the photon possesses a probability to pass straight through it. The probability for photon to penetrate through the pinhole collimator material is determined by the amount of material along the path length of the photon and the particular material.

SIMIND provides routines that sample the initial direction of the photon, the path length of the photon in a particular material and the type of interaction that the photon will undergo when interacting with the material of the pinhole collimator. SIMIND also calculates related energy loss that might have occurred during an interaction. This means that the pinhole collimator routine only has to call SIMIND when it has decided that the photon is about to interact with the material of the pinhole collimator or the photon is about to move in the material of the pinhole collimator.

In the paper by Ljungberg et al. (Ljungberg 1998) a description is given how the direction of a photon and its path length, type of interaction and possible energy loss are calculated.

The direction of a sampled photon and its coordinates when entering the plane of the entrance hole of the knife-edge pinhole insert are for each photon passed to the pinhole collimator routine. When a photon has been processed by the pinhole collimator routine the routine provide the main SIMIND program with the exit coordinate of the photon or with information concerning whether it has been absorbed in the material of the pinhole collimator. This process is repeated until all the photons for a particular projection have been processed.

As SIMIND has been developed in the FORTRAN 90 programming language and so was the pinhole collimator routine and it was constructed as a subroutine to SIMIND.

The pinhole collimator routine

SIMIND samples photons that are processed by the constructed subroutine, more precisely in terms of impact position, initial direction and photon energy. Except for the photon energy, these variables are the incoming variables to the subroutine. The initial position of a photon is confined to the plane of the entrance hole of the knife-edge pinhole insert, and the z-value of its initial position equals the distance, projected onto the z-axis, from the centre of the photon source to that plane of the entrance hole of the knife-edge pinhole insert. The subroutine will process the first position of the photon until the photon reaches the camera head, the photon has been absorbed in the material of the pinhole collimator or its position is outside the pinhole collimator. During the process, the subroutine calls SIMIND routines to sample the type of interactions, if any, that the photon undergoes and its different path lengths during its way through the pinhole collimator, until it reaches the camera head. SIMIND will also keep a record of the energy of the photon.

In general, the pinhole collimator routine examines if the photon is located inside or outside the different compartments of the pinhole collimator. For the inside part of the pinhole collimator; this is done by examine if the position of the photon belongs to one of the sets

given by Equation 7, 8 and 9. For the outside part of the pinhole collimator, it is done by examine if the photon belongs to the one of the sets given by Equation 10, 11 and 12. If the photon does not belong to any of these sets and it does not belong compartment C1 and C5 it is assumed that the photon is inside the material of the pinhole collimator. If the position of the photon is located inside the material of the pinhole collimator, it will interact with the material of the pinhole collimator. If this is the case, the subroutine calls SIMIND routines that sample the type of interaction that will occur, the scatter angle of the photon and its path length, all related to the differential cross-section of the material in question. The routines also calculate an eventual energy loss. SIMIND returns the scatter angle, expressed in direction cosines, and the path length to the subroutine and then the subroutine calculates the new position of the photon with Equation 13.

The following is a description of the underlying principles of the constructed subroutine with the explanation of some details left out-side. The subroutine consists of five block-IF constructions (one for each compartment) nested within a *While* loop. When the photon has reached the surface of the camera head (z equal to z_5), has been absorbed in the material of the pinhole collimator or when the photon has been found to be outside the pinhole collimator, then the *While* loop is terminated. When that happens, the position of the photon is returned to SIMIND.

Each photon that reaches the camera head and the following crystal has been tagged as a geometric, a penetrating or a scattered (in the pinhole collimator) photon during its way trough the pinhole collimator. A photon that is tagged as geometric has passed directly through the aperture without being scattered in the material of the pinhole collimator. A photon that is tagged as penetrating has penetrated through the pinhole collimator without undergoing any interaction. A photon that is tagged as scattered has interacted with the material of the pinhole collimator before reaching the camera head. By using this information, it will be possible to separate events in the image and calculate the fraction of photons that have penetrated or scattered in the pinhole collimator during a simulation.

The first test that is performed using the five block-IF constructions is to decide to which compartment a photon belongs. This is done by comparing the value of the z-coordinate of the current position of the photon with the boundary values of each compartment, defined in Figure 3. When the position of the photon has been located to a compartment, then the block-IF construction that represent the compartment in question continues to examine if the photon is located inside or outside that specific part of the pinhole collimator. If the photon was neither found to be inside nor outside the specific part of the pinhole collimator it is assumed that the photon is inside the material of that part of the pinhole collimator provided that its position did not belong to C1 or C5. Then the subroutine continues to examine if the photon has a positive or a negative z-direction. This decision is made by determining if the value of the *w*-component in the direction cosines of the photon is lager or smaller than zero. If the value of the w-component is equal to zero the *While* loop is halted and a new photon is taken under consideration by the subroutine.

If the photon is found to be inside the pinhole collimator and has a positive *z*-direction the block-IF construction continues to examine if the photon will pass through the exit hole of that specific part of the pinhole collimator. To make this examination possible Equation 13 was rearrange as

$$\begin{cases} x = x' + \dfrac{z - z'}{w} \cdot u \\ y = y' + \dfrac{z - z'}{w} \cdot v \end{cases} \tag{14}$$

where, *z* is the value of the *z*-coordinate of the exit hole, *x* and *y* are the *x*- and *y*-coordinates, respectively, of the photon in the plane of the exit hole. By substituting these coordinates in to

Equation 1 and comparing the calculated radius with the radius of the exit hole in question it is possible to test whether the photon will pas through the exit hole or not.

If the photon has passed through the exit hole, the coordinates of the photon are calculated with Equation 14 and the position of the photon is assigned to theses coordinates and a new turn of *While* loop is started. In the case when the exit hole is the aperture of the knife-edge pinhole insert, the photon is tagged as geometric. In the case when the exit hole is the exit hole of the shielding device, making the photon to strike the lower surface of the camera head, the coordinates of the photon are returned to SIMIND and SIMIND continues to trace the photon inside the camera detector until it escapes or until it has been absorbed.

If the photon does not pass trough the particular exit hole, it is bound to intersect with the inner wall of that specific part of pinhole collimator because of its positive z-direction. If this is the case, the block-IF construction calculates the intersection point between the photon and the inner wall of the pinhole collimator. These calculations were made possible by substituting Equation 14 and the expression of the radius (Equation 2, 3 or 5) into Equation 1 and then solve the quadric equation for z. Since a quadric equation in general has two different solutions, only one of them can represent the correct intersection point between the photon and the inner wall of the pinhole collimator. The correct solution is selected by determining if the largest solution belongs to the compartment in question, i.e. belongs to the z-interval that defines the compartment, or not. If the largest solution belongs to the z-interval, it is the correct one. If instead, the largest solution dose not belonged to the z-interval, the smallest solution is the right one. This is a fact because the photon had a positive direction along the z-axis and its possibility to pass through the exit hole had already been examined. With the correct solution and Equation 14, the x- and y-coordinates of the intersection point are calculated. The calculated intersection point is then assigned as the new position of the photon.

After the intersection point between the photon and the inner wall of the pinhole collimator has been calculated and the photon has been assigned to that position a new path length is sampled**.** Then, with Equation 13, the subroutine calculates the new position of the photon and the block-IF construction continues to examine to which compartment this new position belongs**.** If the new position of the photon is neither found inside nor outside the pinhole collimator the photon is tagged as scattered and a new turn of the *While* loop is stared. In the special case when the photon has intersected with the inner wall of the lower part of the knife-edge pinhole insert (C2) the block-IF construct examines if the new position of the photon is inside the pinhole collimator, or if it is inside compartment 3, 4 or 5. If this is the case the photon, instead of being tagged as scattered, is tagged as penetrating before a new turn of the *While* lope is started.

If the photon instead of being inside the pinhole collimator is determined to be on its outside the *While* loop is halted and a new photon is processed by the subroutine. This is true for all compartments except for compartment 5. If the position of the photon is determined to be inside compartment 5, the pinhole collimator routine tests if the photon has passed through the exit hole of the shielding device, i.e. the photon has passed trough the surface of the camera head. This test was made possible by first substituting Equation 13 in to Equation 1 and then by comparing the calculated radius with the radius of the exit hole of the shielding device. If the photon will pass trough the exit hole of the shielding device the coordinates of the intersection point of the exit hole are calculated with Equation 14 and the intersection point is returned to SIMIND. Then, independent of whether the photon has passed through the exit hole or not, a new photon is processed by the subroutine.

If the position of the photon neither is inside nor outside the pinhole collimator then the block-IF construction examines if the photon has been tagged as scattered or not. If the photon is tagged as scattered the subroutine calls SIMIND to sample the type of interaction that the photon will undergo. SIMIND then returns a new direction and, if Compton scattering is sampled. Then a new path length is sampled and the new position of the photon is calculated with Equation 14 and the *While* loop starts on a new turn. If the photon was not

tagged as scattered its position belongs to the plane, part of the pinhole collimator material, of the entrance hole of the lower part of the knife-edge pinhole insert. If that was the case, a new path length is sampled and a new position of the photon is calculated with Equation 13. If this new position belongs to the inside of the pinhole collimator or it belongs to C5 the photon is tagged as penetrating, else the photon is tagged as scattered. In any case a new turn of the *While* loop is started.

If the photon instead of propagating in a positive *z*-direction is propagating in a negative *z*-direction, the geometry of the pinhole collimator could be thought of as reversed about the *z*-axel. A reversed pinhole collimator means that the same block-IF construction, as in the case of a positive z-direction, can be used. The only difference is how the correct intersection point between the photon and the inner wall o the pinhole collimator is chosen. If the smaller solution to the quadric equation now belongs to the *z*-interval of the specific compartment this is the correct solution, but if it does not belong to *z*-interval of the compartment the larger solution is the correct one.

The flowchart in Figure 14 in the appendix describes the pinhole collimator routine. The position of the photon, (x,y,z_1), and its direction cosine, (u,v,w), enter the routine from SIMIND. Its position in the exit hole of the shielding device is returned to SIMIND, if the *weight* variable is not zero, whenever the logical *loop* variable becomes false. Not that the routine described in Figure 14 in the appendix only handles photons that propagates in a positive z-direction.

Validation of the pinhole collimator routine

It is essential to validate that results from the constructed pinhole collimator routine are in accordance with results obtained from experimental measurements on a clinical pinhole collimator. Therefore, the simulation routine must be evaluated and tested. A way to test the pinhole collimator routine is to compare results from experiments performed on a clinical pinhole collimator with results from corresponding simulations. Another way to evaluate the pinhole collimator routine is to compare results generated with the routine with previously reported results, experimental or simulated.

Results from the pinhole collimator routine were compared with published experimental and simulated results. Several research groups have performed studies on the pinhole collimator. Some have proposed mathematically expressions that describe intrinsic properties of the pinhole collimator, some have investigated the pinhole collimator by analysing it with simulation applications and some have compared experimental results with simulated results.

Monte Carlo simulations programs can be time consuming to construct, run and validate. It took approximately 2 hours, for ten million photons, at the most to generate a planar image when simulating the different systems described below.

Validation by comparison of experiment and simulation

We have validated the pinhole collimator routine by comparing results (from planar images) from simulations with measurements performed on the pinhole collimator at the Biomedical Centre (BMC) at Lund University. The pinhole collimator SPECT system at BMC consists of a SMV DST XLi dual-head scintillation camera system with a mounted pinhole collimator.

The pinhole collimator that was used to validate the pinhole collimator routine consisted of a conical-shaped shielding device, made of lead, and a knife-edge pinhole insert. The interchangeable knife-edge pinhole insert was made of an alloy consisting of 93.0% W, 4.6% Ni and 2.4% Fe with a density of 18 g/cm^3. The diameter of the shielding device at the camera head measured 38.7 cm.

Measurements were performed with a knife-edge pinhole insert with an aperture diameter of 3 mm. With this type of insert, the focal length of the pinhole collimator was 29.5 cm. The

distance between the opening of the knife-edge pinhole insert and the aperture was 1.2 cm and the diameter of the opening measured 1.80 cm. The distance between the aperture and the opening of the knife-edge pinhole insert towards the shielding device was 1.35 cm and the diameter of the opening was 1.95 cm. The diameter of the rim of the knife-edge pinhole insert was 6.0 cm. These measurements were used when simulating the pinhole collimator at the BMC with the constructed simulation routine.

We measured the variation of the system sensitivity (cps/MBq) with distance to the aperture for a point-shaped source located on-axis. The radioactive source that was used was a cylindrical ^{57}Co source with a diameter of approximately 3 mm. The major photon energies, and corresponding abundance, that were used in the Monte Carlo simulations are given in Table 1.

Table 1. Photon energies and relative abundance used in the simulation of the pinhole collimator at BMC.

Radionuclide	Energy (keV)	Abundance (%)
^{57}Co	122.1	85.51
	136.5	10.70
	692.4	0.162

The source was mounted on a plastic bar attached to the couch and centred on the central axis of the pinhole collimator. Measurements were performed with the source placed at a distance of 2.1, 3.1, 4.1 and 5.1 cm from the aperture. The acquisition times were 60, 60, 120 and 240 s, respectively. No correction for decay was necessary. The energy window was set to 20% (FWHM) at 122.1 keV and images were acquired in a 256×256 matrix mode with a pixel size of 0.226 cm.

Normalized sensitivity values were constructed by normalizing the acquired counts in each planar image to the counts in the planar image created at distance of 2.1 cm between the aperture and the source. Normalized point- and line-spread functions (obtained by numerical integration along one direction) were also calculated for each distance between the source and the aperture.

Evaluation by comparison of angle-dependent sensitivity

We have also validated the constructed pinhole collimator routine by comparing results from our simulations with results published by other investigators. Smith et al. (1997) have investigated the angle-dependent sensitivity of a pinhole collimator. They also investigated how the photon penetration through the aperture edge depends on the incident angle of the photon direction. They compared their theoretical and simulated results with experimental results. We have used some of the results in this publication to compare with results generated by the simulation code described in this work.

An important parameter of the knife-edge pinhole insert is the diameter of the aperture, and a change in the diameter will affect the sensitivity, g, of the pinhole collimator. The relative sensitivity of the system is defined as the number of photons that are registered by a scintillation camera as compared to the total number of photons that are emitted from a point

source. Mallard and Myers (1963) have investigated the change of the sensitivity with the distance between a point source and the aperture, and they have proposed the following formula for the sensitivity

$$g = \frac{d^2 \sin^X(\alpha)}{16h^2} \tag{16}$$

where d is the diameter of the aperture, h is the distance between source and the plane of the aperture, and α is the angle between source and the plane of the aperture. The parameter x is here set to 3.

Equation 16 does not take account for the photons that penetrate the edge of the aperture. The penetrating photons make the diameter of the aperture to appear larger than the actual diameter and therefore has an effective diameter, d_e, which can describe this effect, been introduced. Paixs (1967) has proposed the following formula for the effective diameter

$$d_e = \sqrt{d(d + \frac{2}{\mu}\tan\frac{\beta}{2}) + \frac{2}{\mu^2}\tan^2\frac{\beta}{2}} \tag{17}$$

where μ is the linear attenuation coefficient of the material of the knife-edge pinhole insert and β is the acceptance angle of the knife-edge pinhole insert.

The formula for the effective diameter, described by Equation 17, does not include any dependence on the angle between the source and the aperture. A way to model the angle dependency of the sensitivity is to model the exponent of the sine function in Equation 16, i.e. the value of x in $\sin^x(\alpha)$, for a specific aperture diameter and a specific acceptance angle. The angle dependency was modelled in this way by Smith et al. They measured the angular dependency from planar images, as a function of the relative sensitivity, for point sources of ^{99m}Tc and ^{131}I. They estimated the value of x in Equation 16 by fitting a curve to their experimental data, and then the experimental measurements were compared with simulated data. The simulation code used by Smith et al. did not account for scatter within the pinhole collimator and the photon energy was modelled as 140 keV for the ^{99m}Tc point source and 364 keV for the ^{131}I point source. The experiments were performed with four different knife-edge pinhole inserts, made of tungsten, outlined in Table 2. The focal length of the pinhole collimator was 14.5 cm and the distance between the point source and the plane of the aperture was 12.0 cm. During the experiments, the horizontal offsets of the point source were 0, 3, 6, 9 and 12 cm whereas the offsets during corresponding simulations were 0, 2, 4, 6, 8, 10 and 12 cm.

Table 2. Aperture diameters and acceptance angles of the knife-edge pinhole inserts used by Smith et al.

Aperture diameter (mm)	Pinhole insert material	Acceptance angle (degrees)
1.0	tungsten	100
2.0	tungsten	94
3.0	tungsten	88
4.0	tungsten	84

Validation by comparison with penetration and scatter

The photons that constitute the image generated by a pinhole collimator have passed through the aperture of the knife-edge pinhole insert, penetrated the knife-edge pinhole insert or scattered in the pinhole collimator before they reach the detector. The photons that have penetrated the knife-edge pinhole insert and the photons that have been scattered in the pinhole collimator will degrade the image. Therefore, it is of interest to know how different parameters of the pinhole collimator affect the number of penetrating and scattered photons that contribute to the image. It can be of interest to know how these components vary with the origin of the photons, their energy, aperture diameter, acceptance angle and the material of the knife-edge pinhole insert. One way to acquire some knowledge about these variables is to perform simulations.

Deloar et al. (2003) have investigated to which extent penetrating and scattered photons contribute to the picture. Deloar et al. performed simulations on the pinhole collimator described in Figure 5**.**

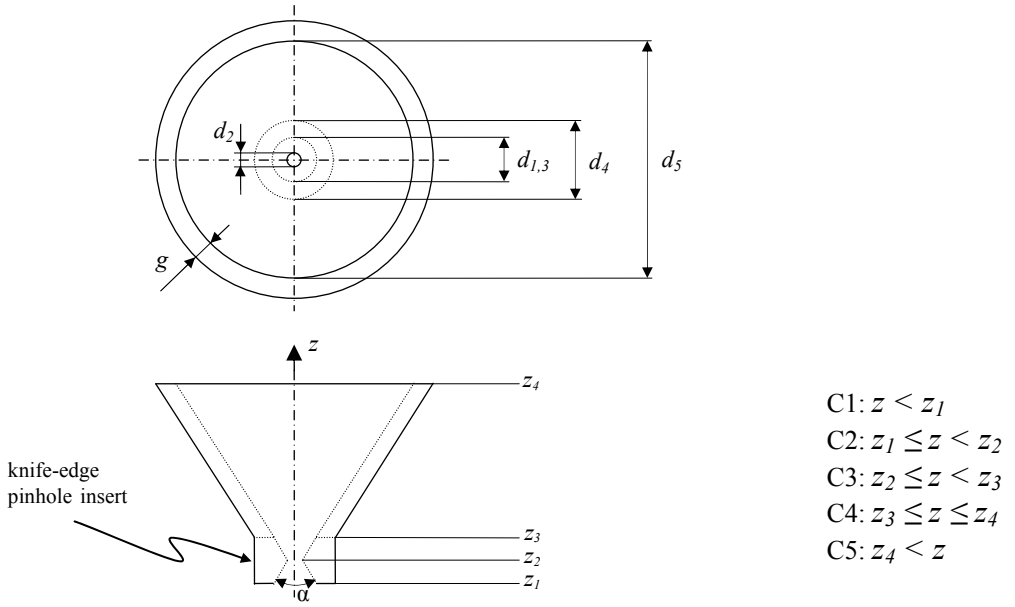

Figure 5. The figure describes the pinhole collimator that Deloar et al. used in the experiments and the simulations that were performed to investigate the relation between penetrating and scattered photons.

In the experiments performed by Deloar, three different knife-edge pinhole inserts made of tungsten were used. All the knife-edge pinhole inserts had an acceptance angle of 60 degrees and the apertures were 1.0, 2.0 and 4.8 mm in diameter. A uniform cylindrical phantom was used (6 cm in length and 4 cm in diameter). Measurements (planar images) were performed with the phantom filled with a solution of either ^{201}Tl, ^{99m}Tc, ^{123}I or ^{131}I. The centre of the

phantom was 4 cm from the centre of the aperture. The energies that were used in the simulations performed by Deloar et al., and their abundance, are tabulated in Table 3 together with the different energy window configurations that were used.

Table 3. Energies, and their distribution, of the radionuclides that were used in the different simulations performed by Deloar et al**.**

Radionuclide	Energy (keV)	Abundance (%)	Energy window (keV)
^{201}Tl	70.8	73.8	70.8 ± 7.08
	167.4	10.0	
	135.5	2.6	
^{99m}Tc	140.5	100	140.5 ± 14.5
^{123}I	159.0	82.2	159.0 ± 15.9
	529.0	1.4	
	538.4	2.7	
^{131}I	364.0	82.0	364.0 ± 18.2

Van der Have et al. (2004) have investigated the relative number of photons that penetrate and scatter in a micro-pinhole collimator. The investigation was performed with a micro-pinhole collimator, described in Figure 6, composed of a 6 mm board with a conical pinhole aperture and a detector that measured 1.63 cm × 1.63 cm.

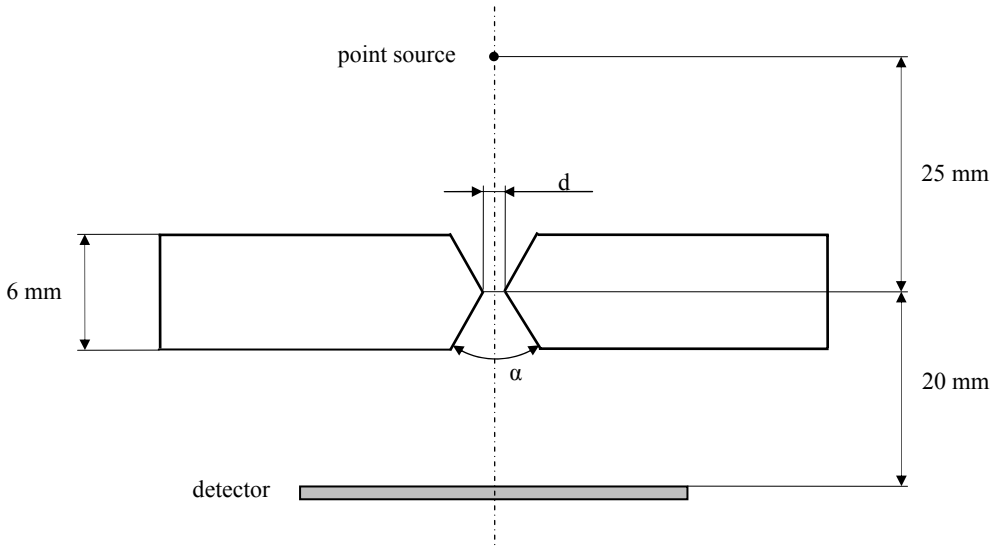

Figure 6. The micro-pinhole collimator used by van der Have. The aperture diameter, *d*, was 100, 300 or 500 μm during the simulations and the acceptance angle, α, was 60 degrees.

Van der Have et al performed simulations with three different micro-pinhole collimators that were made of tungsten, lead, gold or platinum and had aperture diameters of 0.1, 0.3 and 0.5 mm, respectively. The acceptance angle of each micro-pinhole collimator was 60 degrees. A ^{99m}Tc point source was simulated and it was placed on the symmetry axis of the micro-pinhole, 25 mm from the aperture, as shown in Figure 6 above. The energy of the photons

emitted from the simulated source was 140 keV and the energy window was 140±14 keV. We have performed simulations in accordance with the micro-pinhole collimator used by van der Have. Fractions of photons penetrating and scattering in the micro-pinhole collimator were calculated and compared to results published by van der Have et al.

RESULTS

Comparison regarding experimental and simulated spread-function

A comparison between normalized sensitivity calculated from the measurements performed at the BMC and from corresponding simulations performed with the constructed pinhole collimator routine is shown in Figure 7. In Figure 8 to Figure 11 are the point- and line-spread functions calculated that were created when the measurements were performed at the BMC and from the planar images that were created from corresponding simulations.

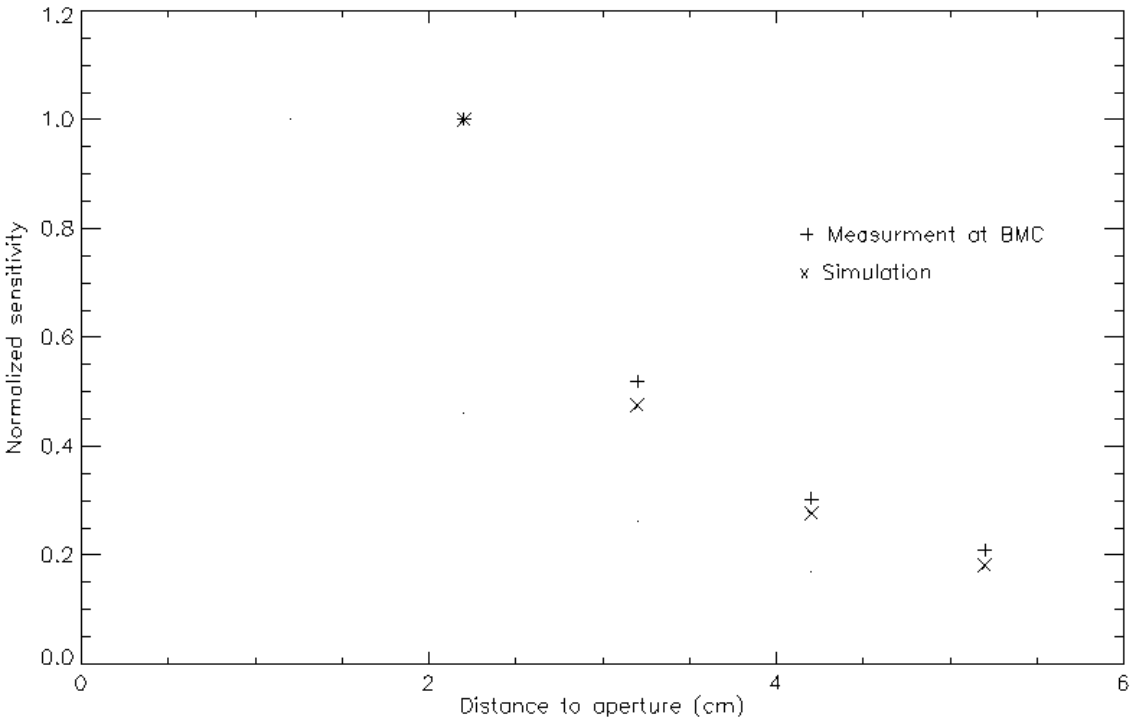

Figure 7. Normalized sensitivity measured at the Biomedical Centre at Lund University (+) and results form corresponding simulations (×).

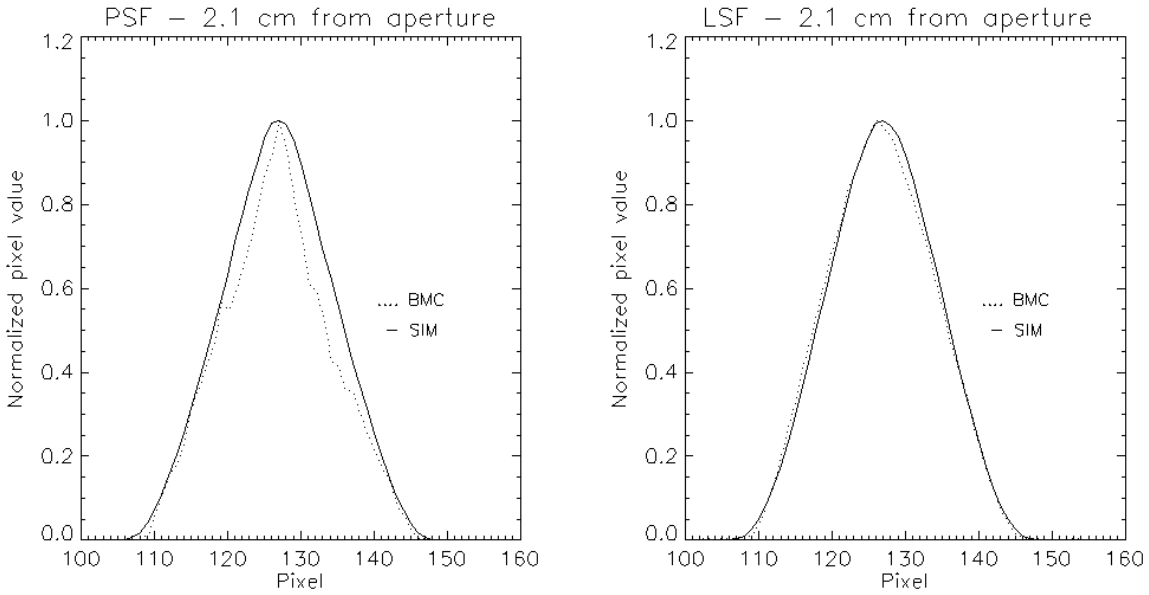

Figure 8. Comparison between simulated and measured point-spread functions (left) and line-spread functions (right) calculated for a distance of 2.1 cm between the source and the aperture. In the left diagram is the experimental (dotted line) compared to the simulated point-spread function and in the right diagram is the comparison between the experimental (dotted line) and the simulated line-spread functions.

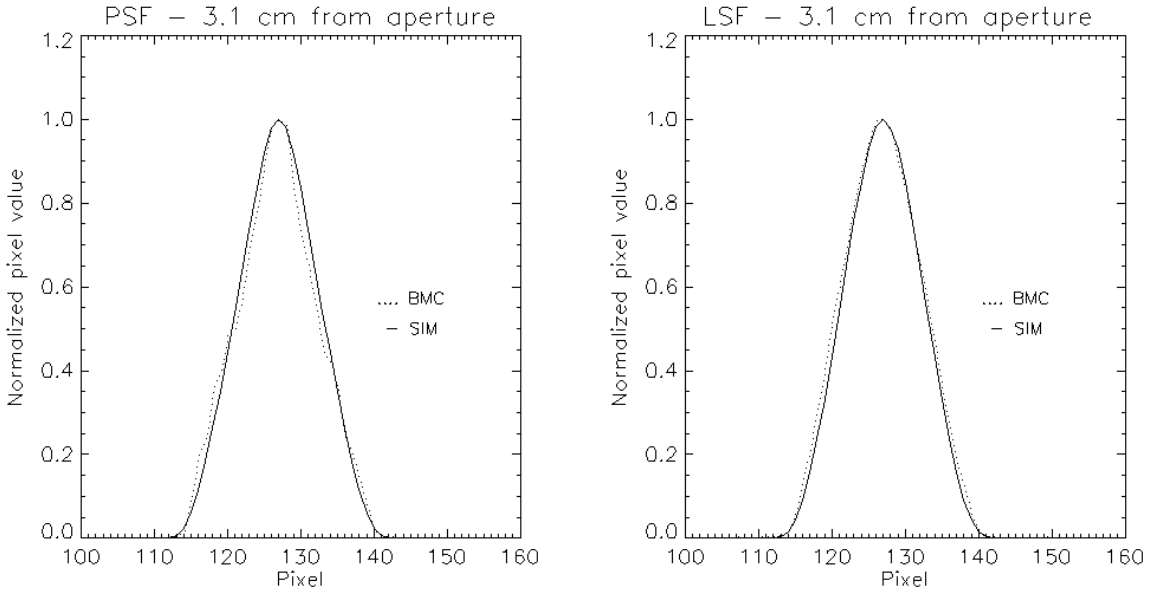

Figure 9. Comparison between simulated and measured point-spread functions (left) and line-spread functions (right) calculated for a distance of 3.1 cm between the source and the aperture. In the left diagram is the experimental function (dotted line) compared to the simulated function and in the right diagram is the comparison between the experimental (dotted line) and the simulated line-spread functions.

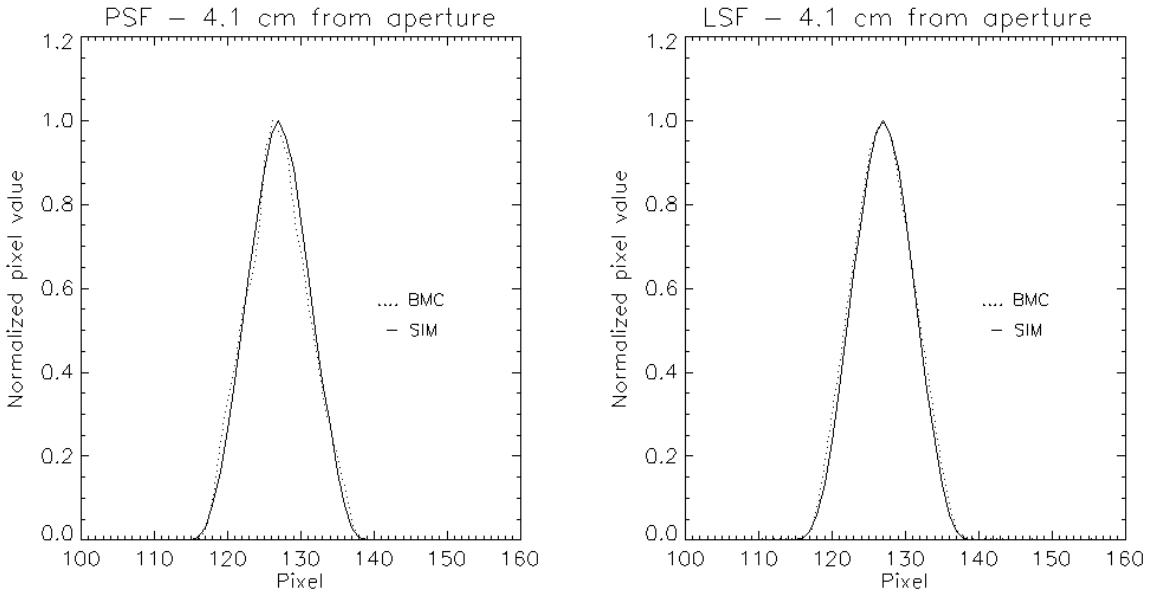

Figure 10. Comparison between simulated and measured point-spread functions (left) and line-spread functions (right) calculated for a distance of 4.1 cm between the source and the aperture. In the left diagram is the experimental function (dotted line) compared to the simulated function and in the right diagram is the comparison between the experimental (dotted line) and the simulated line-spread functions.

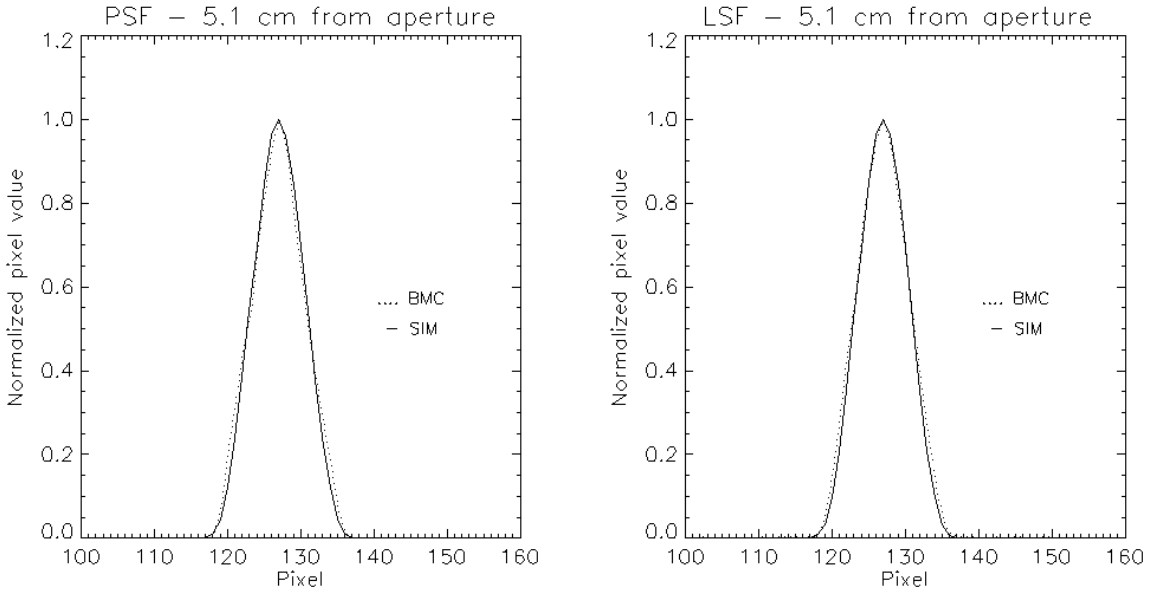

Figure 11. Comparison between simulated and measured point-spread functions (left) and line-spread functions (right) calculated for a distance of 5.1 cm between the source and the aperture. In the left diagram is the experimental function (dotted line) compared to the simulated function and in the diagram right is the comparison between experimental (dotted line) and the simulated line-spread functions.

Comparison regarding angle-dependent sensitivity

Smith et al. (1997) have investigated the sensitivity of the pinhole collimator for different configurations. Table 4 shows a comparison between data published by Smith et al. and corresponding data simulated with the pinhole collimator routine described in this work.

Table 4. Comparison of experimental and simulated angle-dependent sensitivity measured as exponents "x" in Equation 16 (Smith et al. 1997). The right most column shows results simulated with the pinhole collimator routine described in this work.

Aperture diam. (mm)	Acceptance angle (degrees)	Distance to source (cm)	Radionuclide	Smith el al.		This work
				Experimental x	Simulated x	Simulated x
1.0	100	12.0	^{99m}Tc	4.1	4.2	4.2
2.0	94	12.0	^{99m}Tc	3.3	3.8	3.5
3.0	88	12.0	^{99m}Tc	3.5	3.5	3.9
4.0	84	12.0	^{99m}Tc	3.8	3.8	5.2
1.0	100	12.0	^{131}I	7.2	6.9	7.1
2.0	94	12.0	^{131}I	6.3	6.3	6.4
3.0	88	12.0	^{131}I	5.4	5.7	6.8
4.0	84	12.0	^{131}I	5.1	5.4	6.9

Comparison regarding fraction of penetration and scatter

Deloar et al. (2003) have investigated the number of photons that penetrate or scatter in a pinhole collimator. In Table 5 are simulated data published by Deloar et al. presented together with corresponding data generated with the pinhole collimator routine described in this work.

Table 5. Simulated relative numbers of photons penetrating through the knife-edge pinhole insert and photons scattered in the pinhole collimator published by Deloar et al. (2003) compared to corresponding values generated by the pinhole collimator routine presented in this work.

	Aperture diam. (mm)	Deloar et al.				This work			
		^{201}Tl	^{99m}Tc	^{123}I	^{131}I	^{210}Tl	^{99m}Tc	^{123}I	^{131}I
Geometrical (%)	1.0	91.0	75.2	66.8	9.4	78.0	72.3	61.6	4.7
	2.0	95.2	86.2	82.0	23.8	87.7	84.7	78.4	14.8
	4.8	97.7	94.0	92.3	55.1	94.5	93.2	90.5	44.0
Penetration (%)	1.0	3.8	21.0	25.4	74.6	19.0	26.0	34.4	72.3
	2.0	1.8	11.3	14.5	63.6	10.6	14.3	19.7	66.3
	4.8	0.8	5.0	6.4	37.7	4.6	6.3	8.7	45.9
Scatter (%)	1.0	5.2	3.8	7.8	16.0	3.0	1.7	4.0	23.0
	2.0	3.0	2.5	3.5	12.6	1.7	1.0	1.9	18.9
	4.8	1.5	1.0	1.3	7.2	0.9	0.5	0.8	10.1

Van der Have et al. (2004) have investigated the number of photons that penetrate or scatter in a micro-pinhole collimator. In Table 6 are simulated data published by van der Have et al. presented together with corresponding data generated with the pinhole collimator routine described in this work.

Table 6. Experimental and simulated relative numbers of photons penetrating through the micro-pinhole collimator and photons scattered in the micro-pinhole collimator compared to corresponding values generated by the pinhole collimator routine presented in this work.

	Aperture diam. (mm)	van der Have et al.				This work			
		Pb	W	Au	Pt	Pb	W	Au	Pt
Geometrical (%)	0.1	6.56	10.15	12.80	14.27	6.32	9.82	12.45	13.51
	0.3	28.09	36.73	42.02	44.26	27.40	36.06	41.21	43.15
	0.5	43.28	53.00	58.06	60.12	43.25	52.42	57.38	59.13
Penetration (%)	0.1	88.14	84.23	82.27	80.79	85.82	82.28	80.40	79.46
	0.3	68.43	59.90	55.19	53.08	67.43	59.22	54.79	52.98
	0.5	53.54	44.79	40.07	38.12	53.04	44.35	39.94	38.30
Scatter (%)	0.1	5.30	5.62	4.93	4.94	7.86	7.90	7.15	7.03
	0.3	3.48	3.37	2.78	2.66	5.17	4.72	4.00	3.87
	0.5	2.54	2.31	1.88	1.76	3.71	3.23	2.68	2.57

DISCUSSION

The simulated sensitivity as function of distance to aperture shows a good agreement with measured sensitivity, as can be seen in Figure 7, but discrepancies occur. The simulated sensitivity decreases faster in magnitude with distance than the measured. This might be due to uncertainties in the measurements when placing the ^{57}Co source on the symmetry axis of the pinhole collimator or uncertainties in the measurements of the source-collimator distance. For example, if the source is positioned an additional 2 mm away from the aperture then the simulated sensitivity values yield a better fit to the measured sensitivity than the simulated sensitivity shown in Figure 7. However, if the source is moved 3 mm instead of 2 mm fore every position, the simulated sensitivity starts to deviate from the measured data. The simulated sensitivity will also be different for a 2 mm error in the horizontal direction but this error will however, not have the same impact on the results. For future comparisons between measurements and simulations of the sensitivity is it therefore essential to develop an accurate procedure to place the source on the symmetry axis of the pinhole collimator and to measure the distance between the source and the aperture with a high precision.

Since it is possible to separate photons passing through the aperture from the rest of the photons that have been detected during a simulation session, it was possible to compare calculated results from Equation 16 with results from the simulations of the sensitivity, in this case with a ^{57}Co point source. The geometrical sensitivity obtained by simulation decreased as a function of the inverse of the squared source-to-aperture distance, just as Equation 6 predicts. This result indicates that the pinhole collimator routine correctly describes the imaging characteristics related to the aperture but it does not prove any accuracy of the number of photons that penetrate or scatter in the pinhole collimator.

The simulated point- and line-spread functions in Figure 8 to Figure 11 agree very well with corresponding measured functions. The line-spread functions resemble data best but the figures show some differences that might be related to the accuracy in which the source dimension, the focal length, the source-to-aperture distance and the offset of the source relative to the symmetry axis could be measured.

When moving the source away from the aperture, the width of the spread functions will decrease and if a bigger source is used the width of the spread functions will increase. A small

offset of the source from the symmetry axis will widen the spread functions but the effect will diminish as the source is moved away from the aperture. The width of the spread-function will also increase with the focal length of the pinhole collimator as the magnification of the pinhole collimator increases with the (length of) the focal length. The size of the source was not a great problem to establish. It was easily measured with a vernier calliper. However, it had to be assumed that the radioactive material was distributed homogeneous throughout the source.

As discussed above, the distance between the aperture and the source was not measured with any special means neither was it confirmed that the couch, to which the source was attached, moved in precise steps of 1 cm and that it moved along the symmetry axis of the pinhole collimator.

Thus, the most significant source-of-error of the measurements is probably the error in the distance between the aperture and the source. The distance between the source and the aperture was measured with a ruler that only had a millimetre scale, and the error of a measurement could therefore have been in the order of a millimetre. The uncertainties when measuring the source dimensions was small. However, because of the magnification of the pinhole collimator, even a small error in the diameter of the source would have affected the measured point- and line-spread functions. The error in the focal length was approximated to a millimetre, which is 0.3% of the focal length.

The comparisons with simulated angular dependency measured by Smith el al. for ^{99m}Tc and ^{131}I sources show good agreement for acceptance angles of 100 and 94 degrees but for acceptance angles of 88 and 84 degrees they are not good, as can be seen in Table 4.
In the work by Smith et al., the source was initially placed on the symmetry axis. Then the source was moved away from the symmetry axis in consecutive steps of 3 cm until it was 12 cm from the symmetry axis. At this distance from the axis and for an acceptance angle of 84 or 88 degrees for a knife-edge pinhole insert the source is nearly on the edge of (or even outside) the Field-of View for the pinhole collimator. The shape of the source and the design of the knife-edge pinhole insert will then become critical for the outcome of a measurement of the sensitivity. Smith et al. did however, not specify any dimensions of the knife-edge pinhole insert that were used during the experiments other than the aperture diameter and the acceptance angle. Because of this, we have used the geometry of the knife-edge pinhole insert at BMC when simulating the sensitivity.

The sensitivity at the edge of the field of view will vary with the thickness of the knife-edge pinhole insert, i.e. the distance *h* from the aperture to the bottom (and the top) as illustrated in Figure 12. The distance between the aperture and the top and bottom of the knife-edge

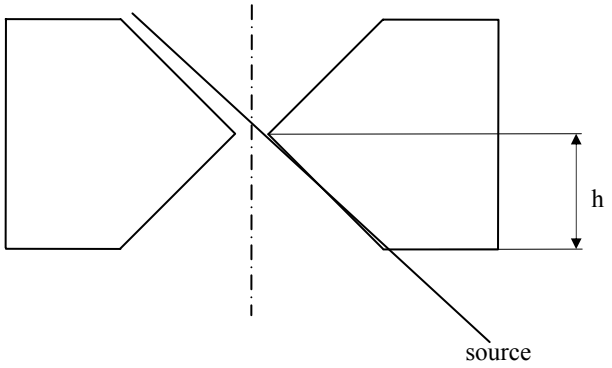

Figure 12. The figure illustrates how a photon either pas through the aperture of a knife-edge pinhole insert or not, depending on the measurement of the distance, *h*, between the aperture and the top and bottom of the knife-edge pinhole insert.

pinhole insert can of course assume different values depending on design of the knife-edge pinhole insert. Despite this fact simulations with the same distance between the aperture and the top and the bottom of the knife-edge pinhole insert were performed, with values of *h* ranging from 0.7 to 1.3 cm. The exponent, x, in Equation 16 became smaller for the knife-edge pinhole insert that had acceptance angles of 84 and 88 degrees as *h* was decreased, while the exponent almost stayed constant fore the knife-edge pinhole inserts that had acceptance angles of 94 and 100 degrees. Even though the exponents came closer to the exponents given by Smith et al. in Table 4 as *h* was increased they never were a perfect match.

The exponent *x* may not only depend on the value of *h* but also on the interface between the knife-edge pinhole insert and the shielding device. If the entrance hole of the shielding device has the same diameter as the exit hole of the knife-edge pinhole insert, the sensitivity will be less than for a situation where an entrance hole has a larger diameter than the diameter of the exit hole of the knife-edge pinhole insert. The diameter of the exit hole of the shielding device will only have a minor influence on the sensitivity. It will only start to affect the sensitivity when the knife-edge pinhole insert becomes so thin, or the photon energy is so high, that it will no longer prevent radiation from penetrating at the interface between the shielding device and the knife-edge pinhole insert.

Smith et al. used 3 mm of a capillary tube filled with radioactive solution as a source. During the simulations, the capillary tub hade a radius of 1.5 mm and a length of 3 mm, which probably made the source larger than the source used by Smith et al. Simulations were also performed with a point source but the resultant sensitivity did not change much compared to the sensitivity measured with a capillary tube as a source. (*The size of the source did therefore not have a significant effect on the sensitivity*.)

Because of the uncertainty of the dimensions of the pinhole collimator, it is hard to say if the pinhole collimator routine simulates a pinhole collimator in an accurate way. However, as long as the source is kept inside the field-of-view of the pinhole collimator the routine simulates a pinhole collimator in a correct way according to the comparisons that were made with the measurements performed by Smith et al.

The comparison between our results and the results of the fraction of photons passing through the aperture, penetrating its edge or scattering in the knife-edge pinhole insert calculated by Deloar et al. as is shown in Table 5, is not god in a quantitative way. This is especially true for the comparison between relative numbers of photons that scatter in the knife-edge pinhole insert. Still the comparison is good in a qualitative way, i.e. the number of photons that penetrate or scatter in the knife-edge pinhole insert decrease with the diameter of the aperture.

The comparison of relative number of photons that pass through the aperture, penetrate its edge or scatter in the pinhole collimator measured by van der Have et al. in Table 6, is not good in a quantitative way but the comparison is better than the comparison in Table 5. These differences might have been caused by the use of different attenuation tables and different tables of probabilities for a photon to interact with the material of the pinhole collimator. However, there are of course other possibilities.

There is a difference in geometry between the simulations that were performed by Deloar et al. and van der Have et al. While van der Have et al simulated a point source Deloar et al. simulated a cylindrical source, with a uniformly distributed solution of ^{99m}Tc, in which the photons could loose energy by Compton scattering. This energy loss could have affected the probability for a photon to penetrate the edge of the aperture, which in turn would have affected the relative amount of photons that penetrated or scattered in the pinhole collimator.

The increasing interest for small-animal imaging also for SPECT has justified a development of a pinhole collimator routine also for the virtual camera. The main advantage here is to be able to optimize pinhole collimator parameters, such as hole-diameters and geometrical properties of the insert to obtain the best image quality.

As an example of an application with the pinhole collimator simulation Monte Carlo simulation using the develop routine can produce very realistic images when using the Moby

mouse computer phantom (Segars et al, 2004). A preliminary result of such simulation is shown in Figure 13 where the three images to the left show simulated projections using three different apertures and the right image shows an image of the mouse. These images are some of several SPECT projections around the mouse, which are reconstructed to transversal slices using a special cone-beam Feldkamp reconstruction method.

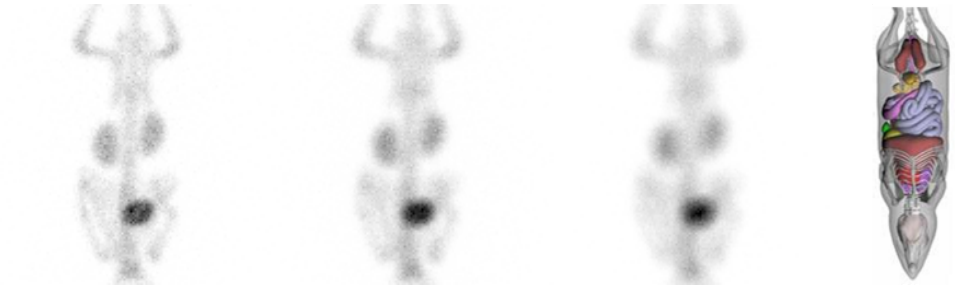

Figure 13. The above three images are projections from a virtual camera with a pinhole collimator with 1, 2 and 3 mm aperture. Right image shows the mouse phantom and the different organs segmented.

CONCLUSION

A SIMIND based pinhole-imaging simulation application was constructed and evaluated. The application was constructed to simulate pinhole collimator consisting of a knife-edge pinhole insert and a conical shielding device mounted on a SPECT system. The application was validated through comparison between experiments performed on a SPCECT system with a mounted pinhole collimator and corresponding simulations. Comparisons between simulations and previously reported results were also performed to validate the application. The validation shows that the application describes a pinhole-imaging device. However, the comparison with previously reported results shows that there are uncertainties in the relative number of photons that pass through the aperture, penetrate its edge or scatter in the pinhole collimator. Therefore must comparisons with more prices experiments be performed before the application can be approved as a functional pinhole-imaging application. Except fore further comparison with experiments, the constructed routine has to be completely integrated with the “change” program.

Appendix

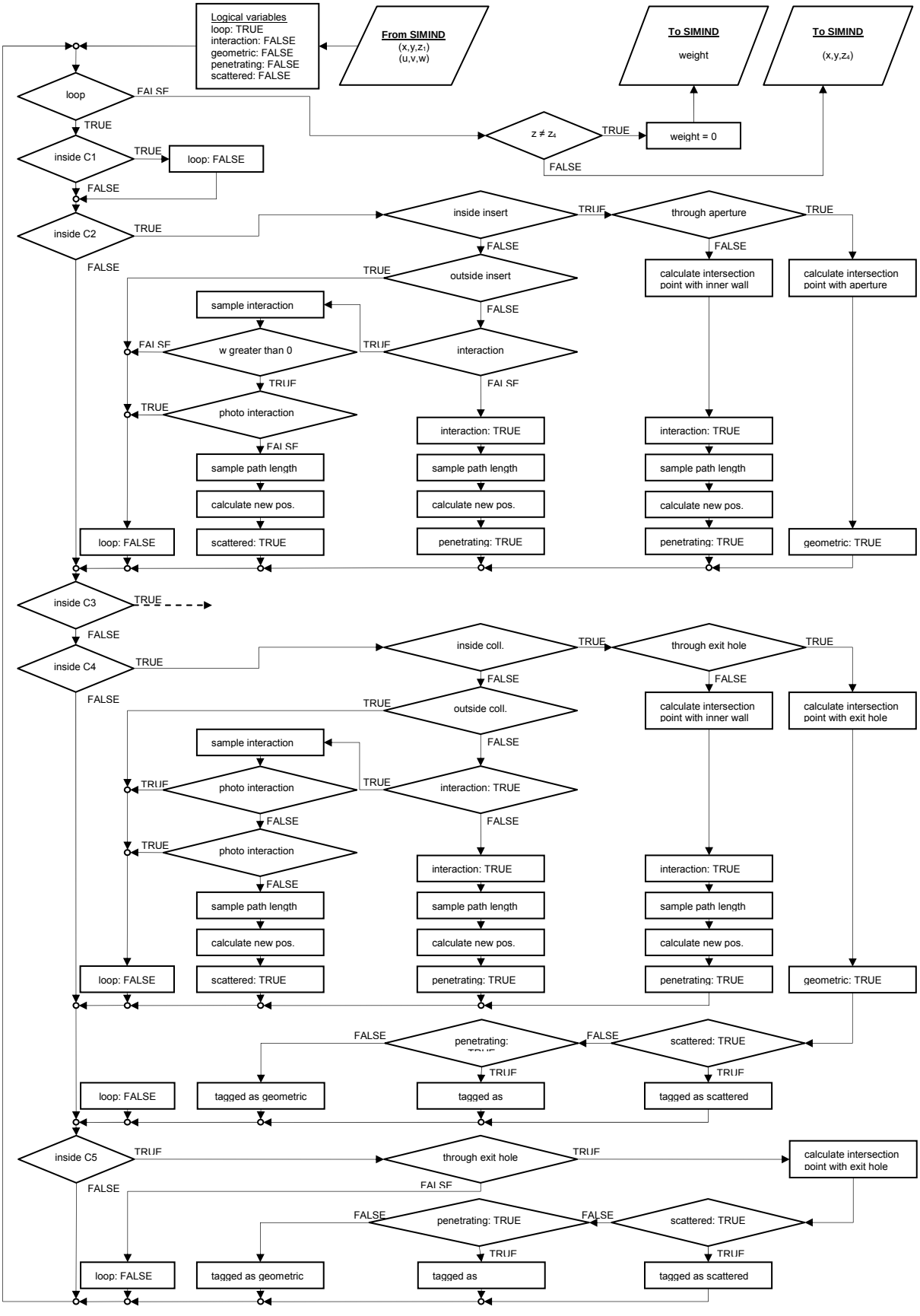

Figure 14. The flowchart describes how the pinhole collimator routine works. The abbreviations pos. stands for position and coll. stands for collimator. The process that follows if the photon is found inside C3 processes the photon in the same way as the process that follows if the photon is found inside C1.

REFERENCES

Hossain M Deloar et al., Evaluation of penetration and scattering components in conventional pinhole SPECT: phantom studies using Monte Carlo simulations. Phys. Med. Biol. 48 995-1008. 2003.

Ljungberg, M., The SIMIND Monte Carlo program. Ljungberg, M., Strand, S.-E., and King, M. A. Monte Carlo Calculation in Nuclear Medicine: Applications in Diagnostic Imaging, 145-163. 1998. Bristol and Philadelphia, IOP Publishing

Mallard J R and Myers M J, The performance of a gamma camera for the visualization of radioactive isotopes in vivo. Phys. Med. Biol. 8 165-182. 1963.

Paix, D., Pinhole Imaging of Gamma Rays, Phys. Med. Biol. 4 489-500, 1967.

Segars W. P., Tsui B. M. W., Frey E. C., Johnson G. A. , Development of a 4D digital mouse phantom for molecular imaging research. Molecular Imaging & Biology, vol. 6, no. 3, pp. 149-159, 2004.

Smith Mark and Jaszczak Ronald, The effect of gamma ray penetration on angle-dependent sensitivity for pinhole collimator in nuclear medicine. Med. Phy. 24 (11). 1997.

C.R. Tenny et al., Uranium Pinhole Collimators for I-131 SPECT Brain Tumor Imaging. IEEE 1999.

van der Have and Freek J Beekman, Photon penetration and scatter in micro-pinhole imaging: a Monte Carlo investigation. Phys.Med Biol. 49. 2004.